

Optimization of Surface Plasmon Excitation Using Resonant Nanoparticle Arrays above a Silver Film

Amitabh Ghoshal, Pieter G. Kik

CREOL: College of Optics and Photonics, University of Central Florida, 4000 Central Florida Blvd., Orlando, FL 32816

ABSTRACT

A plasmonic coupling device consisting of an array of ellipsoidal silver nanoparticles embedded in silica in close proximity to a silver surface is studied. By tuning the inter-particle spacing, the shape of the particles in the array, and the height of the array above the silver film, the array-mediated surface plasmon excitation is studied. Finite Integration Technique simulations of such a plasmon coupler optimized for operation at a free space wavelength of 676 nm are presented. Plane wave normal incidence excitation of the system results in resonantly enhanced fields near the nanoparticles, which in turn excite surface plasmons on the metal film. The existence of an optimum particle-surface separation for maximum surface plasmon excitation efficiency is demonstrated. Analysis of the frequency dependent electric field in the simulation volume as a function of particle aspect ratio reveals the influence of the particle resonance and the surface plasmon resonance on the excitation efficiency.

Keywords: surface plasmon, nanoparticle array, resonance, anti-crossing

1. INTRODUCTION

In recent years, there has been a tremendous amount of research in surface plasmon nanophotonics. Surface plasmons are collective oscillations of charge density that occur at a metal-dielectric interface or at a metal surface.¹ Surface plasmon modes can be strongly confined, and as a result surface plasmon waveguides are considered to be a possible candidate for densely integrated photonic circuits.²⁻¹⁰ Recently several viable designs have been demonstrated. These include metal stripes¹¹, wedges⁵, and gaps⁴ in metal films, and strip-loaded surface plasmon waveguides². Passive surface plasmon based components have been developed, including Bragg reflectors¹², ring resonators¹³, and Y-splitters¹³. Active components such as Mach-Zehnder interferometer based switches¹⁴ have been also realized. A crucial component for integrated optical circuits based on surface plasmons is an integrated light source; however no viable surface plasmon source has yet been developed. As a result, surface plasmon based circuits require optical coupling elements that allow addressing of nanophotonic devices using far-field optics.

Far-field excitation of surface plasmons is challenging due to the mismatch between the free-space wavelength of light and the surface plasmon wavelength at a metal-dielectric interface. A common method of exciting surface plasmons is prism coupling in either the Kretschman¹ or the Otto¹ geometry. In this approach the wavevector of the incident light is increased using a high refractive index material in close proximity to the metal surface. The excitation efficiency using these methods can be close to unity using broad area illumination. A second method of surface plasmon excitation is grating coupling, which also allows for close to unity excitation efficiency if extended gratings are used.¹ Here the momentum mismatch between free-space light and the surface plasmon is overcome by the grating momentum. A third method of surface plasmon excitation involves the use of sub-wavelength features on a metal surface. For example, a near-field scanning optical microscope tip can be used to excite surface plasmons locally.¹⁵ Surface plasmon excitation by light incident on random surface roughness¹⁶, as well as intentionally created features such as metal nanoparticles¹⁷ and lines¹⁷ on or near^{18, 19} a metal film, holes in metal films²⁰⁻²², and edges of metal films²³ has also been demonstrated.

In this study we numerically investigate excitation of surface plasmons in a silver film using a 2-dimensional array of ellipsoidal silver nanoparticles placed in close proximity to a silver surface. We evaluate the effect of the inter-

particle separation in the longitudinal (x) direction, the particle resonance, and the particle-surface separation on the efficiency of surface plasmon excitation at the Ag surface.

2. DEVICE STRUCTURE AND SIMULATION DETAILS

We investigate a structure consisting of a two dimensional array of ellipsoidal silver nanoparticles in close proximity to a silver surface. The response of the system to electromagnetic illumination was simulated using the Finite Integration Technique (FIT)^{24, 25} with commercially available software CST Microwave Studio. A silver film of thickness 200 nm, and extended infinitely in the x - y plane, was embedded in SiO₂. This thickness was chosen to prevent significant coupling of surface plasmon amplitude from the top to the bottom surface of the silver film. An ellipsoidal silver nanoparticle of semi-axes $a \times b \times c$ in the x , y , and z -directions respectively was embedded in the

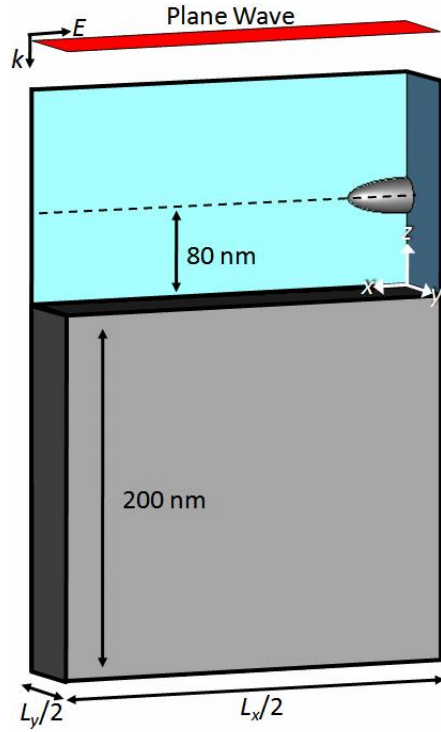


Figure 1. Schematic of the simulation volume.

silica with the center of the nanoparticle positioned 80 nm above the metal surface for all calculations except in the array-surface distance dependent calculations. The system was illuminated using a plane wave polarized along the x -direction and travelling along the negative z -direction. The temporal dependence of the excitation signal was a Gaussian modulated sine wave centered at a free-space wavelength of 676 nm (4.35×10^{14} Hz) and a pulse duration of 16 fs, which corresponds to a wavelength range from 451 nm (6.65×10^{14} Hz) to 1357 nm (2.21×10^{14} Hz). The center wavelength was chosen to correspond to a wavelength of a Kr-ion laser. However, the system is expected to behave similarly at communication wavelengths such as 850 nm, with a further reduction in losses, and a corresponding shift in the resonance frequencies described below. The lateral particle-particle spacing was set to $L_y = 100$ nm, and the longitudinal particle-particle spacing was set to $L_x = 440$ nm, which corresponds to the calculated surface plasmon wavelength at a Ag-SiO₂ interface for a free-space wavelength of 676 nm. A schematic of the simulation volume is shown in Figure 1. Pseudo-periodic boundary conditions were implemented in the x and y -directions by setting the tangential electric field to zero at $x = 0$ and at $x = L_x/2$, and setting the tangential magnetic fields to zero at $y = 0$ and $y = L_y/2$. These parameters effectively simulate an infinite array of nanoparticles with a longitudinal spacing of L_x and a lateral spacing of L_y above an infinitely extended silver film. Open boundary conditions were used at the positive and negative z -boundaries. The dielectric constant of silver was described using the modified Drude model

$$\epsilon_r = \epsilon_\infty - \frac{\omega_p^2}{\omega(\omega - i\Gamma)} \quad (1)$$

where ϵ_r is the relative permittivity of the silver, $\epsilon_\infty (= 4.03783)$ is the dielectric constant of the metal at infinity, $\omega_p (= 1.3807 \times 10^{16}$ rads/s) is the plasma frequency, and $\Gamma (= 1.1171 \times 10^{13}$ Hz) is the damping frequency of the material. The real part of the permittivity was found to be within 6% of the experimental data²⁶ across the bandwidth used, and the imaginary part of the permittivity was set to the experimental value at the design frequency. Due to the non-Drude like behavior of the damping in silver, deviations up to 80% were present at the extreme frequencies. The dielectric constant of silica was set to a constant value of $\epsilon_r = 2.21$.

Mesh cell sizes between 1-4 nm were used in the regions of high field variation in the simulation volume to ensure mesh convergence of the results. Mesh convergence tests show that the errors in the electric field magnitude and resonance frequency values in the remainder of this work are $\pm 2.5\%$ and $\pm 0.2\%$ respectively.

3. SIMULATION RESULTS

Figure 2 shows the obtained distribution of the z component of the electric field (E_z) in the x - z plane at $y = 0$, for an ellipsoidal particle with an aspect ratio (AR) of 3.5 at the frequency $f = 4.35 \times 10^{14}$ Hz. The vertical component of the electric field is seen to change sign around the film surface, which implies the presence of a surface charge indicative of a surface plasmon. Around the nanoparticle evidence for a predominantly dipolar mode is found, although partly masked by the presence of strong surface related field components. The charge distribution of both

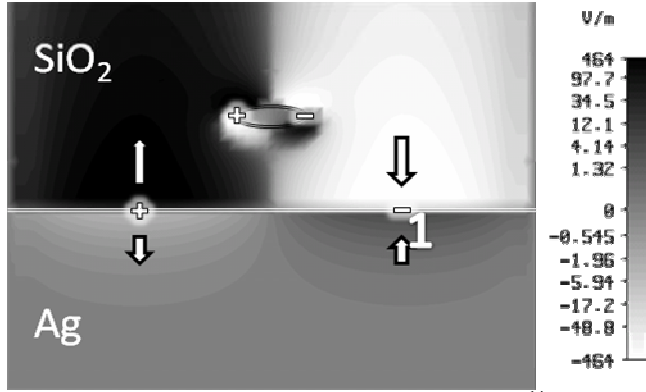


Figure 2. E_z fields at $y = 0$ at a frequency of 4.35×10^{14} Hz. The + and - signs schematically indicate the location of charges and the arrows indicate the directions of the fields.

the surface plasmon mode and the dipolar particle mode is sketched schematically by the + and - signs in Figure 2. In order to evaluate the excited surface plasmon amplitude, we monitor the E_z amplitude at position 1. Note that at this position, the particle dipole field adds an E_z contribution. The time evolution of the E_z signal at location 1 is shown in Figure 3 (bottom panel). Although the excitation signal ends at time 0.016 ps (top panel), extended ringing of the electric field is observed after the excitation has ended, indicating the existence of electromagnetic resonances of the system. Figure 4 displays the Fourier Transform of this time-domain signal, normalized to the Fourier Transform of the incident pulse. Two clear resonances are observed. The resonance at 4.35×10^{14} Hz approximately coincides with the analytically calculated frequency

of 4.44×10^{14} Hz for a silver-silica surface plasmon with a wavelength of $\lambda_{SP} = L_x$. Consequently, this resonance is attributed to the constructive excitation of surface plasmons along the x -direction as excited by the nanoparticle grating, and is referred to as the surface plasmon resonance. The resonance observed at 3.7×10^{14} Hz lies close to the numerically calculated nanoparticle resonance frequency of 3.81×10^{14} Hz for an isolated silver particle of an AR of 3.5 embedded in silica. Note that since the signal shown in Figure 4 is normalized to the excitation signal Fourier Transform, the field amplitudes larger than 1 are indicative of local field enhancement.

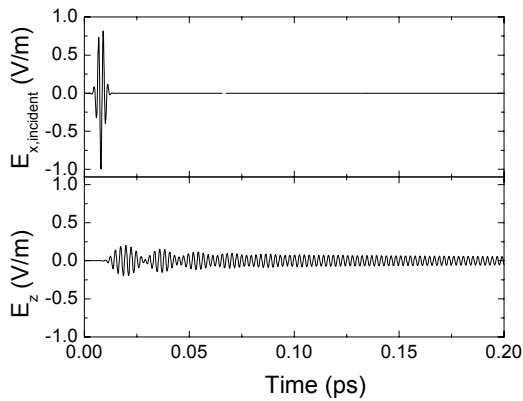


Figure 3. Top: excitation signal monitored at the port. Bottom: Time evolution of the E_z field at location 1.

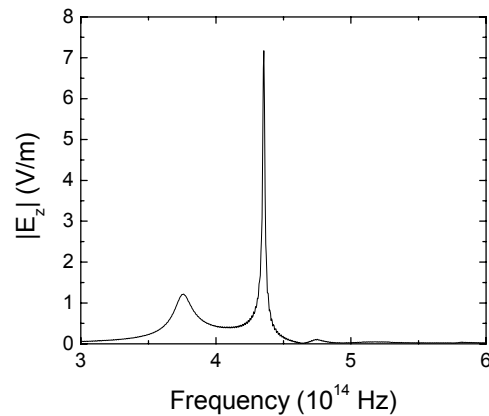


Figure 4. Fourier Transform of the time domain E_z signal at location 1.

The frequency dependent field amplitude as shown in Figure 4 was calculated as a function of inter-particle distance in the x -direction, particle aspect ratio, and array-to surface distance.

We first examine the effect of varying the longitudinal inter-particle spacing while keeping the particle aspect ratio at 2.5 and the array-surface distance at 80 nm. The inter-particle spacing was varied from 400 nm to 500 nm, in steps of 20 nm, and the results are shown in Figure 5. A sharp resonance peak is observed for all simulations, and is again attributed to the constructive excitation of propagating surface plasmons. The resonance feature observed at approximately 4.6×10^{14} Hz lies close to the analytically calculated nanoparticle resonance frequency for a particle with $AR = 2.5$. Separate simulations of an isolated silver particle of the same dimensions in SiO_2 also exhibit this resonance peak, confirming that this resonance is particle related. The surface plasmon peak is seen to shift from 4.75×10^{14} Hz to 3.75×10^{14} Hz as the inter-particle distance is changed from 400 nm to 500 nm. From the simulations, the FWHM of the particle resonance is found to be $3 \times 10^{13} \text{ s}^{-1}$, and the FWHM of the surface plasmon resonance is $2 \times 10^{12} \text{ s}^{-1}$. The amplitude of the surface plasmon resonance is seen to reach a maximum of 7.6 V/m at a longitudinal particle spacing of $L_x = 440$ nm. The occurrence of maximum surface plasmon amplitude at frequencies below the single particle resonance is most likely due to a balance between excitation efficiency and radiative loss: for strong particle-film interaction, any excited amplitude can rapidly dissipate in the form of free-space radiation. At frequencies away from the particle resonance, excited SP amplitude will not couple efficiently to the nanoparticle, resulting in a longer effective SP lifetime. At frequencies above the particle resonance frequency, the particle amplitude is reduced, as is typical of any resonator, resulting in reduced surface plasmon excitation strength.

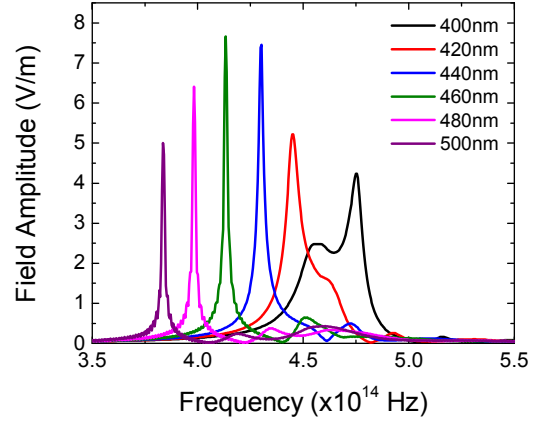


Figure 5. E_z at location 1 for L_x ranging from 400 nm to 500 nm, at an aspect ratio of 2.5.

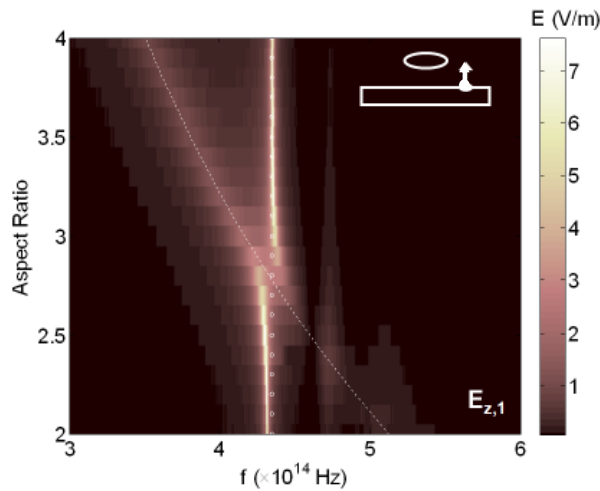


Figure 6. Electric field strength of oscillations in the frequency range 3×10^{14} Hz to 6×10^{14} Hz at location 1 as measured in the simulations. The color represents the magnitude of the relevant component of the electric field.

The nanoparticle resonance is seen to decrease from 5.4×10^{14} Hz to 3.6×10^{14} Hz. The dashed white line in Figure 6 marks the independently calculated resonance frequency of an isolated silver nanoparticle of the same aspect ratio embedded in SiO_2 . As the particle resonance approaches the surface plasmon resonance, a shift in the surface plasmon resonance as well as the particle resonance is observed. This type of anti-crossing is typical of strongly coupled resonant systems.

To study the influence of the interaction strength of the nanoparticle array with the incident field, the aspect ratio (defined as a/c) of the particle was varied from 2 to 4 while keeping the volume constant and equal the volume of a 15 nm radius spherical nanoparticle. The calculation shown in Figure 4 was repeated for particle aspect ratios in the range of 2-4 (in steps of 0.1) corresponding to single particle resonance frequencies in the range 5.1×10^{14} Hz to 3.5×10^{14} Hz. The results are shown in Figure 6. The color represents the magnitude of the electric field response at each frequency and aspect ratio, and the corresponding electric field amplitudes are indicated by the color bar. The location of the silver-silica surface plasmon resonance at 4.35×10^{14} Hz is indicated by the vertical dotted line.

As the aspect ratio of the particle increases, the resonance frequency of the feature associated with the surface plasmon resonance shifts as well as the particle resonance is observed. This type of anti-crossing is typical of strongly coupled resonant systems.

NOTE: Corrected Fig. 6. The original graph displayed E_x data instead of E_z data.

Finally, to study the behavior of the system as a function of array-surface separation, we examine two sets of simulations, one set at $AR = 2.5$ and another set at $AR = 3.5$, while changing the array-surface distance from 15 nm to 200 nm. Figure 7 shows the z -component of the time domain electric field at location 1 for the various array-surface spacings, both for $AR = 2.5$ (Figure 7(a-e)) and 3.5 (Figure 7(f-j)). Note that a maximum in the (instantaneous) field amplitude is observed at a separation of 50nm. Surprisingly, the SP amplitude is found to drop to near-zero values at a particle height of 15 nm. This result is most likely due to a combination of strong radiative loss, a change in the particle resonance frequency due to interaction with the film, and a reduced spatial overlap between the dipolar particle field and the surface plasmons at these small spacings.

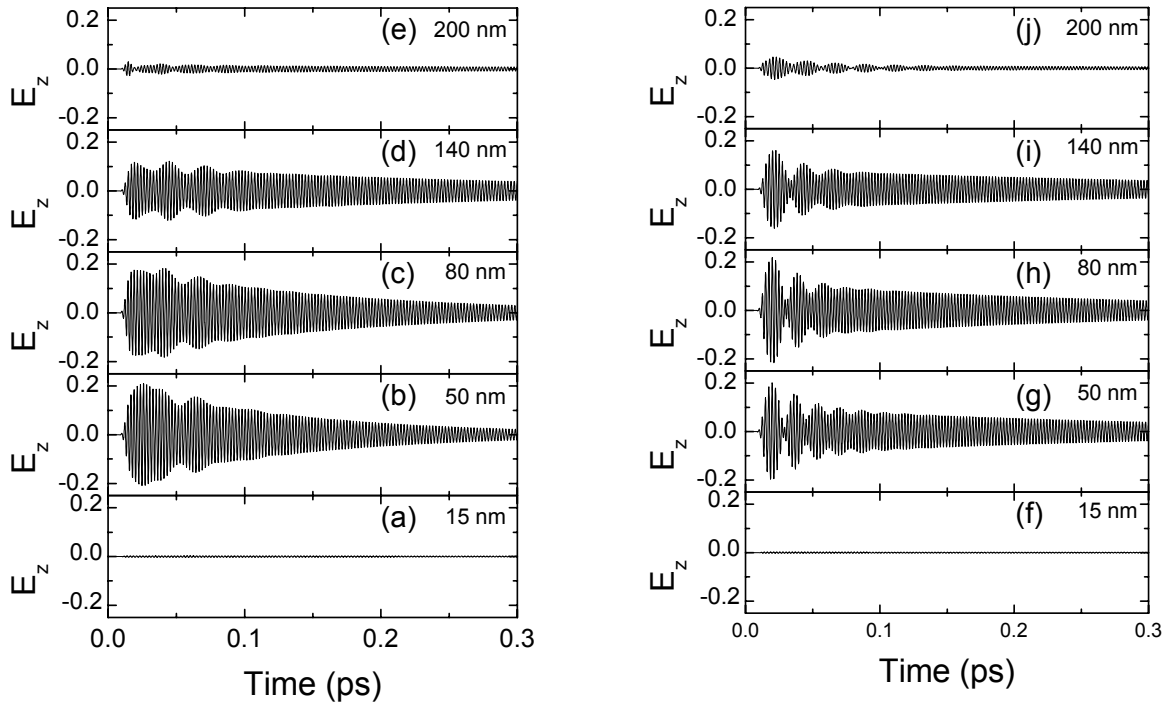


Figure 7. Time dependence of the E_z field at location 1 for various particle-film separations. The height of the center of the particle is indicated in each graph. Graphs (a)-(e) correspond to $AR = 2.5$, and graphs (f)-(j) correspond to $AR = 3.5$.

The peak amplitude of the surface plasmon resonance obtained from the Fourier transforms of the time domain signals at location 1 is shown as a function of particle-film separation in Figures 8(a) and (b). The two particle shapes produce a remarkably similar behavior: as the array-surface separation is increased from 15 nm to 50nm, a strong increase in the amplitude of the excited surface plasmon is observed. As the separation is increased from 50nm to 150 nm, the field amplitude remains relatively constant. As the separation is increased further the surface plasmon amplitude gradually decreases. For both aspect ratios an optimum field amplitude is observed at a particle-film separation of approximately 80 nm. The similarity of the results obtained for particles with $AR = 2.5$ and $AR = 3.5$ is surprising. As can be seen from Fig. 6 (particle-surface separation 80nm) an AR of 2.5 corresponds to SP excitation below the nanoparticle resonance, while an AR of 3.5 corresponds to SP excitation well above the particle resonance. It is expected that these findings are the result of the distance and AR dependent field overlap of the nanoparticle field with the SP field distribution and vice-versa, as well as the intrinsic AR -dependent nanoparticle damping. Although further work is needed, it seems likely that the observations are linked to the

existence of low damping in the surface resonance and the requirement of small particle-film separations for near-field excitation of surface plasmons.

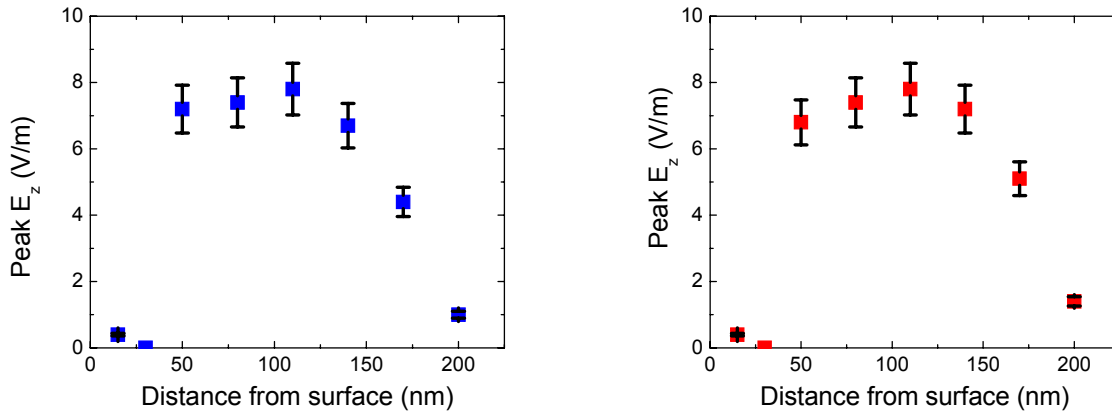


Figure 8. Peak E_z value of the surface plasmon resonance for as a function of particle-film separation, showing (a) results for AR = 2.5, and (b) results for AR = 3.5. The error bars are representative of the inaccuracy of the calculations as described in section 2.

4. CONCLUSION

We have performed FIT simulations to study the behavior of an array of silver nanoparticles embedded in silica above a silver film under normal incidence plane wave illumination. The simulation results show strong coupling which is observed as anti-crossing of the resonant features of both the individual particles, and of surface plasmons at the Ag-SiO₂ interface. The simulations indicate the presence of an optimum particle-surface separation of 80 nm for maximum surface plasmon excitation. The optimum spacing appears to be relatively independent of particle aspect ratio in these particular infinitely extended structures. The simulation results suggest that the optimization of the surface plasmon excitation efficiency in such resonant systems requires a balance between the intrinsic damping and the radiative loss.

REFERENCES

1. Raether, H., "Surface Plasmons on Smooth and Rough Surfaces and on Gratings", Springer Tracts in Modern Physics. Vol. 111, Springer-Verlag, Berlin, 1998.
2. Steinberger, B., et al., "Dielectric stripes on gold as surface plasmon waveguides", Applied Physics Letters, **88**(9), p. 094104, 2006.
3. Krenn, J.R., et al., "Non diffraction-limited light transport by gold nanowires", Europhysics Letters, **60**(5), p. 663-669, 2002.
4. Pile, D.F.P., et al., "Two-dimensionally localized modes of a nanoscale gap plasmon waveguide" Applied Physics Letters, **87**(26), p. 261114, 2005.
5. Gramotnev, D.K. and D.F.P. Pile, "Single-mode subwavelength waveguide with channel plasmon-polaritons in triangular grooves on a metal surface", Applied Physics Letters, **85**(26), p. 6323-6325, 2004.
6. Pile, D.F.P. and D.K. Gramotnev, "Channel plasmon-polariton in a triangular groove on a metal surface", Optics Letters, **29**(10), p. 1069-1071, 2004.
7. Leosson, K., et al., "Long-range surface plasmon polariton nanowire waveguides for device applications", Optics Express, **14**(1), p. 314-319, 2006.
8. Nikolajsen, T., et al., "Polymer-based surface-plasmon-polariton stripe waveguides at telecommunication wavelengths", Applied Physics Letters, **82**(5), p. 668-670, 2003.

9. Dionne, J.A., et al., "Plasmon slot waveguides, Towards chip-scale propagation with subwavelength-scale localization", *Physical Review B*, **73**(3), p. 035407, 2006.
10. Krenn, J. and J. Weeber, "Surface plasmon polaritons in metal stripes and wires", *Philosophical Transactions of the Royal Society A, Mathematical, Physical and Engineering Sciences*, **362**(1817), p. 739-756, 2004.
11. Weeber, J.-C., Y. Lacroute, and A. Dereux, "Optical near-field distributions of surface plasmon waveguide modes", *Physical Review B (Condensed Matter and Materials Physics)*, **68**(11), p. 115401, 2003.
12. Krenn, J.R., et al., "Surface plasmon micro- and nano-optics", *Journal Of Microscopy-Oxford*, **209**, p. 167-172, 2003.
13. Bozhevolnyi, S.I., et al., "Channel plasmon subwavelength waveguide components including interferometers and ring resonators", *Nature*, **440**(7083), p. 508-511, 2006.
14. Nikolajsen, T., K. Leosson, and S.I. Bozhevolnyi, "Surface plasmon polariton based modulators and switches operating at telecom wavelengths", *Applied Physics Letters*, **85**(24), p. 5833-5835, 2004.
15. Webb-Wood, G., A. Ghoshal, and P.G. Kik, "In situ experimental study of a near-field lens at visible frequencies", *Applied Physics Letters*, **89**, p. 193110, 2006.
16. Fang, N., et al., "Regenerating evanescent waves from a silver superlens", *Optics Express*, **11**(7), p. 682-687, 2003.
17. Ditlbacher, H., et al., "Efficiency of local light-plasmon coupling", *Applied Physics Letters*, **83**(18), p. 3665-3667, 2003.
18. Ghoshal, A., et al., "Coherent far-field excitation of surface plasmons using resonantly tuned metal nanoparticle arrays", *Proc. SPIE*, **5927**, p. 255-262, 2005.
19. Papanikolaou, N., "Optical properties of metallic nanoparticle arrays on a thin metallic film", *Physical Review B*, **75**(23), p. 235426, 2007.
20. Jin, E.X. and X. Xu, "Radiation transfer through nanoscale apertures", *Journal of Quantitative Spectroscopy and Radiative Transfer*, 2004. **93**(1-3), p. 163.
21. Thio, T., et al., "Enhanced light transmission through a single subwavelength aperture", *Optics Letters*, **26**(24), p. 1972, 2001.
22. Guo Ping, W., Y. Yongxiang, and W. Bing, "Evanescent coupling of transmitted light through an array of holes in a metallic film assisted by transverse surface current", *Journal of Physics, Condensed Matter*, **15**(47), p. 8147, 2003.
23. Sarid, D., "Long-range surface-plasma waves on very thin metal films", *Physical Review Letters*, **47**(26), p. 1927, 1981.
24. Weiland, T., "Eine Methode zur Losung der Maxwellschen Gleichungen fur sechskomponentige Felder auf diskreter Basis", *AEU*, **31**, p. 116-120, 1977.
25. Weiland, T., "Ein allgemeines Verfahren zur Berechnung elektromagnetischer Felder und seine Anwendung in Physik und Technik", *DESY*, **106**, p. 1-37, 1986.
26. Johnson, P.B. and R.W. Christy, "Optical Constants of the Noble Metals", *Physical Review B*, **6**(12), p. 4370-4379, 1972.
27. Ditlbacher, H., et al., "Fluorescence imaging of surface plasmon fields", *Applied Physics Letters*, **80**(3), p. 404-406, 2002.